Unlocking the Potential of Xylooligosaccharides: Nanofiltration for Efficient Fractionation of Hardwood Hydrolysates

Gloria Lizeth Diaz-Arenas [a], Huy Quoc Hoang [a], Hans Cainglet [a], M. Munir Sadiq [b], Gil Garnier [a], Joanne Tanner [a*]

[a] *Bioresource Processing Research Institute of Australia (BioPRIA), Department of Chemical and Biological Engineering, Monash University, Clayton, VIC 3800, Australia*

[b] *Manufacturing, CSIRO, Clayton, VIC 3169, Australia*

*Joanne Tanner (Corresponding Author); **E-mail address:** joanne.tanner@monash.edu

Full postal address: *Woodside Building for Technology and Design, Room 328, 20 Exhibition Walk, Monash University, Clayton, VIC, Australia*

Abstract

Xylooligosaccharides (XOS) are oligomers constituted of 2 to 10 xylose units derived from xylan-rich lignocellulosic biomass. These oligomers possess significant value in biotechnological and functional food applications, which are determined by their degree of polymerization (DP), and the type and number of substituents. Separation of XOS is industry-specific, and it presents a formidable challenge for large-scale production due to their complexity and similarity. This study investigated the use of nanofiltration membranes to fractionate beechwood-xylan hydrolysates containing XOS. Tubular ceramic membranes with molecular weight cut-offs (MWCO) of 750, 450 and 200 Da were able to separate XOS into three distinct DP ranges namely, high (X2-X5), medium (X2-X4) and low (X2-X3), respectively. The impacts of operating pressure and pH were evaluated to select the conditions leading to high permeate flux while maintaining high rejection of X6, X5 and X4 for the 750, 450 and 200 Da membranes, respectively. The trade-off between XOS rejection and flux was favored at pH 7.0 for the 750 and 450 Da membranes, pH 4.2 for the 200 Da, and operating pressure of 10 bar for the three membranes. These results demonstrate the feasibility of nanofiltration for large-scale separation of XOS with specific properties.

Keywords: Fractionation; Glucuronoxylan; Hemicellulose; Nanofiltration; Xylooligosaccharides.

Abbreviations

BCA	Bicinchoninic acid
CIP	Cleaning-in-place
DP	Degree of polymerization
ELSD	Evaporative light scattering detector
HPLC	High performance liquid chromatography
LC-Q-TOF-MS	Liquid chromatography coupled with quadrupole time-of-flight mass spectrometry
MWCO	Molecular weight cut-off [g/mol]
OP	Operating pressure [bar]
SLM	Standard liter per minute
TMP	Transmembrane pressure [bar]
X1	Xylose
X2	Xylobiose
X3	Xylotriose
X4	Xylotetraose
X5	Xylopentaose
X6	Xylohexaose
XOS	Xylooligosaccharides

Nomenclature

$C_{i,f}$	Concentration of compound *i* in the feed [mg/L]
$C_{i,p}$	Concentration of compound *i* in the permeate [mg/L]
L_p	Permeability [LMH/bar]
J	Permeate flux [LMH]
R_i	Rejection of compound *i* [%]

Greek Letters

ρ	Density [kg/L]
τ	Turbidity [cm^{-1}]

1. Introduction

Bioactive molecules such as xylooligosaccharides (XOS) have gained attention in recent years for applications in functional foods, medicines, and phytopharmaceuticals [1]. The XOS are produced by chemical or enzymatic hydrolysis of xylan-rich hemicellulosic biomass and are composed of xylose (X1) units linked by β-(1-4)-xylosidic bonds with degrees of polymerization (DP) from 2 to 10 [2]. Enzymatic hydrolysis is preferred over chemical hydrolysis as it limits the generation of products such as monosaccharides and their dehydration to furfural and hydroxymethylfurfural [3]. The hydrolysates resulting from enzymatic hydrolysis comprise a mixture of XOS with various DPs, types and degrees of substitution, which determine their biotechnological applications [4]. Studies have reported that XOS with DP 2-3 show prebiotic, antioxidant and antibacterial activities [1, 5, 6], while XOS with DP ≥ 4 show stabilizing, thickening and emulsifying properties [7]. As a result, refining hydrolysates into XOS with specific DP is important in the application of XOS and to meet the industry standards for high-purity XOS (75-95%) [8].

A variety of downstream techniques have been evaluated to refine XOS, including adsorption by surface-active materials, solvent extraction, and chromatography [9]. However, these techniques are not feasible or cost-effective for large-scale production of XOS [10]. Membrane technology offers a promising approach for the separation and purification of XOS due to its inherent scalability, compatibility with existing industrial processes, ability to operate in continuous mode, and high processing capacity [11].

The earliest reports of refining oligosaccharides using membrane technology date back to the early 2000s using ultrafiltration and nanofiltration membranes [3, 10, 12]. Ultrafiltration results in more polydisperse fractions and the use of membranes with low molecular weight cut-off (MWCO) is recommended to minimize the dispersion of molecular sizes [13]. For XOS, ultrafiltration (MWCO 1 - 50 nm) is more suitable as a pre-treatment step for the removal of high molecular weight oligomers and enzymes, rather than for obtaining a highly purified product consisting of short-chain oligosaccharides [14]. In contrast, nanofiltration (MWCO < 2 nm) is effective in producing high-purity XOS (92% to 96% purity) [15, 16]. Vegas *et al.* [15] reported a multistep process using a ceramic membrane with MWCO of 1 kDa in combination with solvent extraction and ion exchange could remove monosaccharides and non-saccharide compounds while retaining XOS with a purity of 92%. Gullón *et al.* [12] evaluated tubular ceramic membranes with MWCO of 50, 15, 5, and 1 kDa to refine XOS from autohydrolysis of *Eucalyptus globulus* wood, retaining 85% of XOS with 1 kDa membrane. However, none of these studies reported the range of DP of the purified XOS mixture.

Zhao *et al.* [16] used a spiral wound membrane with MWCO of 250 Da in diafiltration mode to remove xylose and arabinose from corncob and wheat straw syrups containing XOS with DP 2-6. The concentrated XOS contained 96% of XOS, and the xylose and arabinose content decreased from 13.39% to 3.05%, and 2.83% to 0.85%, respectively. In a more recent study, low molecular weight XOS (DP 2-3) were fractionated from sugarcane straw hydrolyzed liquor using nanofiltration membranes with MWCOs of 500-600 Da (NP030, polyethersulfone) and 200-300 Da (TS40, polypiperazine amide) in a dead-end filtration system. The optimal pH, temperature, and pressure for both membranes were determined but information on fouling after hydrolysate filtration and membrane performance after different cycles was not provided [7].

Separation efficiency, *i.e.,* selectivity and permeate flux, is directly influenced by membrane features (geometry and material), process conditions, and oligosaccharide composition (molecular weight, type and degree of substitution, and structural conformation) [17, 18]. The biggest challenge when working with membrane technology, is fouling, which adversely impacts membrane selectivity and reduces permeability [19]. The primary mechanisms of membrane fouling are concentration polarization and pore blockage, which can lead to reversible or irreversible fouling [12]. Physical or chemical cleaning can restore membrane performance lost due to fouling [20, 21]. Ceramic membranes are particularly appealing due to their ability to withstand harsh environments, including exposure to chemicals, mechanical stress, and high temperatures [22]. These membranes can be regenerated through chemical cleaning, making them a durable and cost-effective option for industrial applications [23].

The aim of this study is to fractionate hydrolysates into three XOS ranges named high (X2 to X5), medium (X2 to X4), and low (X2 and X3) DP using ceramic nanofiltration membranes with MWCOs of 750, 450, and 200 Da. The hydrolysates used in this study were produced via enzymatic hydrolysis of beechwood xylan. The effects of filtration parameters including operating pressure (5, 10, and 15 bar) and hydrolysate pH (4.2, 7.0, and 10.0) on the separation performance were evaluated to select the best conditions in the trade-off between selectivity and permeate flux for the three XOS ranges.

2. Materials and Methods

2.1 Chemicals and reagents

Commercial beechwood xylan (product code BI3856) was purchased from Apollo Scientific. Acetonitrile (catalogue number 100030), ammonia solution 25% (catalogue number 543830), citric acid monohydrate (catalogue number 100242), sodium citrate dihydrate (catalogue number W302600), and sodium hydroxide (catalogue number 106469) were obtained from Sigma-Aldrich. Endo-1,4-β-xylanase from *Thermomyces lanuginosus* (≥2500 U/g), expressed in *Aspergillus oryzae* (EC 3.2.1.8) (catalogue number X2753), and xylose (catalogue number PHR2102, 99%, X1) were acquired from Sigma-Aldrich. Xylobiose (product code O-XBI, X2), xylotriose (product code O-XTR, X3), xylotetraose (product code O-XTE, X4), xylopentaose (product code O-XPE, X5), and xylohexaose (product code O-XHE, X6) with the purity > 95% were purchased from Megazyme. Ultrapure water (18.2 MΩ-cm at 25 °C) was generated by a Millipore Milli-Q Advantage A10 water purification system (Darmstadt, Germany).

2.2 Hydrolysate

The hydrolysates used in this study were produced via enzymatic hydrolysis of beechwood xylan (glucuronoxylan) using endo-1,4-β-xylanase in sodium citrate buffer 50 mM. Xylose yield-limiting parameters of the enzymatic hydrolysis were determined in a previous study [24], and used in the present work. Those parameters resulted in hydrolysates with a complete XOS profile and correspond to xylan concentration of 3.0% w/v, enzyme dose of 20 mg enzyme per mL of the reaction mixture, citrate buffer pH 4.0, the reaction time of 90 min and an incubation temperature of 25 °C. Briefly, 50 mL of the reaction mixture was equilibrated at 25 °C before adding the endo-1,4-β-xylanase and placing it in an incubator shaker (Infors Ecotron, Bottmingen, Switzerland) at 230 rpm.

The reaction was quenched by immersing the hydrolysates in a water bath (Thermoline Scientific, Sydney, Australia) at 100 °C for 10 min (deactivating enzyme). Next, the hydrolysates were centrifuged at 10,000 rpm for 5 min, and the supernatant was taken. The resulting hydrolysates were boiled again for 10 min, and 10-fold diluted with ultrapure water to minimize the osmotic pressure over the membrane [25]. Then, the diluted hydrolysates were vacuum filtered using 0.45 μm mixed cellulose ester membranes (Advantec MFS Inc, Tokyo, Japan) before filtration experiments to remove any macromolecules (protein) and to limit membrane fouling. The quantitative composition of the 10-fold diluted and prefiltered hydrolysates is presented in **Table 2**. For the filtration experiments, the default pH of the diluted hydrolysates was 4.2 and it was adjusted with 4 M sodium hydroxide depending on the evaluated pH (7.0 or 10.0).

2.3 Membranes

Single-channel tubular ceramic membranes of 1000 mm in length, inner diameter of 7 mm, and outer diameter of 10 mm were purchased from Inopor® (Scheßlitz, Germany) with the molecular weight cut-offs (MWCOs) of 750, 450, and 200 Da in the range of nanofiltration. The support layer of the membranes was made out of α-Al_2O_3, and the active layer was made of TiO_2. Detailed information on the membranes is presented in **Table 1**. To prepare the membranes for further use, a diamond saw was utilized to carefully cut them, resulting in a final effective membrane area of 0.0021 m^2. The membrane ends were sealed using Araldite® 2020 resin (Product code 00052144) following the manufacturer's instructions.

2.4 Filtration system

A crossflow filtration system from Nanjing Tangent Fluid Technology Co. Ltd (TFT) (Nanjing, China) was modified and customized for operation with a tubular membrane module of 11.4 cm in length. **Fig. 1** shows the configuration of the filtration system which consisted of a 12 L jacketed feed tank, a plunger diaphragm pump followed by a damper to reduce pulsations, pressure gauges before and after the membrane module to measure the transmembrane pressure (TMP), and a flowmeter to measure the recirculation flow. The temperature was controlled by circulating water into the jacket of the feed tank using a refrigerated bath circulator (Thermoline Scientific, Sydney, Australia). Filtrations were performed in recycle mode using 2.5 L of feed solution (ultrapure water, sodium hydroxide solution, or hydrolysate). All experiments were conducted at 25 °C unless otherwise stated, and the operating pressures (OPs) were selected to ensure the safety range of TMP recommended by the membrane manufacturer (**Table 1**).

Table 1. Detailed information on the nanofiltration membranes including molecular weight cut-offs (MWCOs), temperature range, transmembrane pressure (TMP) and pH ranges provided by the manufacturer.

Membrane	MWCO	Porosity	Temperature range [°C]	TMP [bar]	pH range
Nanofiltration	750 Da	30 - 40%	0 - 300	8 - 15	0.5 - 14
	450 Da	30 - 40%	0 - 300	8 - 15	0.5 - 14
	200 Da	30 - 40%	0- 150	8 - 15	0.5 - 14

MWCO: Molecular weight cut-off, TMP: Transmembrane pressure.

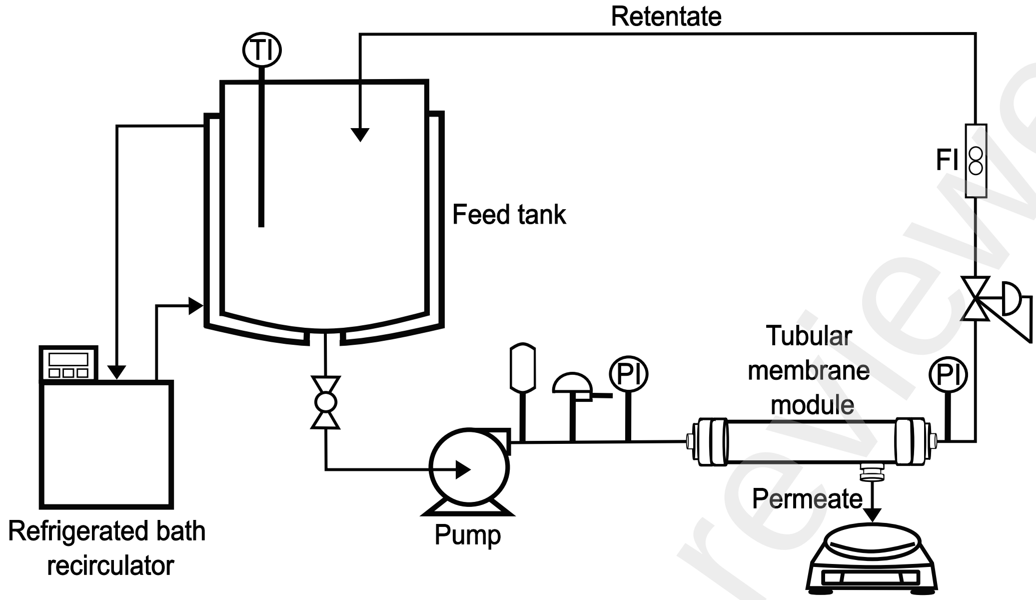

Fig. 1. Schematic representation of the crossflow filtration system customed for a tubular membrane module. The feed solution is pumped from the feed tank to the membrane module using a plunger diaphragm pump. The retentate is recycled to the feed tank, and the permeate is collected in a beaker placed on a weighing scale.

2.5 Filtration experiments

2.5.1 Cleanging-in-place

After the cutting and sealing procedures, a cleaning-in-place (CIP) protocol was implemented to remove any possible dust or dirt within the membranes. The cleaning protocol consisted of two steps: (1) circulation of 1% w/v sodium hydroxide at 40 °C for 60 min at OP of 5 bar while recycling the permeate; (2) rinsing the membranes with ultrapure water at 25 °C and OP of 5 bar until reaching neutral pH in the permeate. The cleaning protocol was also performed after each filtration experiment of hydrolysates to remove any build-up of protein or oligomers on the surface or pore structure of the membranes. The effectiveness of CIP was assessed by measuring pure water flux after membrane cleaning and prior to hydrolysate experiments. The pure water fluxes were recorded for the 750, 450, and 200 Da membranes after 30 min of equilibration time at 25 °C, OP of 5 bar, and the results of ten cycles are presented in **Fig. S1.**

2.5.2 Permeability measurement

The pure water and hydrolysate permeate fluxes were measured using the crossflow filtration system for each nanofiltration membrane. The permeate collector beaker was placed on a weighting balance (Mettler Toledo, Greifensee, Switzerland) connected to a PC running the LabX Direct Balance Software (version 2.5). Data collection started after setting the OP, and permeate steadily flowed to the collector beaker. The LabX Direct Balance Software recorded the mass change in the beaker as a function of time. The steady-state permeate flux (J, L h^{-1} m^{-2} or LMH) was calculated using Eq. (1) [26], where ΔM is the change in mass of liquid permeated within a given time interval Δt, ρ is the density of the liquid at 25 °C, and A is the effective membrane area.

$$J = \frac{\Delta M}{\rho A \, \Delta t} \quad \textbf{(1)}$$

Permeability (L_p) (LMH/bar) was calculated using Eq. (2) [27], where TMP is the transmembrane pressure (bar).

$$L_p = \frac{J}{TMP} \quad \textbf{(2)}$$

2.5.3 Influence of pressure on selectivity and flux

For each membrane, the influence of the OP on the selectivity and permeate flux (J) was evaluated using the diluted and prefiltered hydrolysate as feed. The evaluated OPs were 5, 10 and 15 bar, the feed was kept at 25 °C, and filtrations were carried out for 60 minutes. To ensure a constant concentration in the feed, the collected permeate was returned to the feed tank every 15 minutes. At the beginning of each filtration, feed samples were collected, while permeate and retentate samples were taken every 15 minutes throughout the experiment. This procedure was implemented to monitor the concentration in the feed tank and the permeate and evaluate the membrane performance over time.

For each OP, permeate flux (*J*) was calculated (Eq. (1)) and the collected samples were used to measure the concentration of each XOS by HPLC-ELSD. The selectivity of the membranes for a given compound was expressed by the rejection coefficient (*R*) [28], which was determined from the concentration of each compound *i* in the permeate (C_p) and feed (C_f) solutions using Eq. (3) [29]:

$$R_i = \left(1 - \frac{C_{i,p}}{C_{i,f}}\right) \times 100 \quad \textbf{(3)}$$

2.5.4 Influence of pH on selectivity and flux

The influence of pH on the selectivity and permeate flux (*J*) was investigated by varying the pH of the hydrolysate feed. The hydrolysate pH was adjusted from 4.2 (default) to 7.0 and 10.0 using a 4 M sodium hydroxide solution, the feed was kept at 25 °C, and filtrations were carried out for 60 minutes. Sampling was conducted as described in section *2.5.3*.

2.5.5 Statistical analysis

The results of the filtration experiments using the three nanofiltration membranes at various operating pressures and hydrolysate pH values were analyzed by Student's *t*-test using Minitab 17 software (Minitab Inc., State College, USA). The results were presented as the mean ± standard deviation (SD) and the $p < 0.05$ was considered statistically significant.

2.6 Analytical methods

2.6.1 Xylose and xylooligosaccharides quantification

An Agilent Technologies 1260 Infinity ll HPLC system coupled to an evaporative light scattering detector (ELSD) (Agilent Technologies, Palo Alto, USA) was used to analyze the feeds, retentates and permeates collected at the different sampling times for each filtration experiment. The separation was carried out on a Shodex HILICpak VG-50 (4.6 × 150 mm) chromatographic column (Showa Denko America, New York, USA). Samples were filtered using a 0.2 µm Acrodisc® syringe filter (Pall Corporation, Port Washington, USA) and 10 µL were injected via a vial-sampler onto the column. The mobile phase was an aqueous solution with 0.1% v/v ammonia [solvent A] and HPLC-grade acetonitrile [solvent B]. The target analytes were separated at 50 °C at a flow rate of 0.7 mL min^{-1} in gradient elution mode as follows: 80% [B] held for 1 min, 80-65% [B] in 17 min, 65% back to 80% [B] in 6 min, 80% [B] held 11 min. The ELSD evaporator and nebulizer temperatures were set at 70 °C at a nitrogen gas flow rate of 1.5 SLM. Instrument control, data acquisition and processing were conducted using OpenLab CDS software, version 2.6 (Agilent Technologies, Santa Clara, USA). The target analytes were quantified using the external standard calibration method by preparing a 6-point calibration curve at defined concentrations for X1-X6 standards. Commercial standards for linear XOS with DP > 6 and branched XOS were unavailable but their identity was confirmed by liquid chromatography coupled with quadrupole time-of-flight mass spectrometry (LC-Q-TOF-MS) using the conditions described in **Appendix A** (Supplementary Data).

2.6.2 Enzyme concentration

The enzyme concentration in each membrane's feed, retentate and permeate was determined using the Novagen® bicinchoninic acid (BCA) Protein Assay Kit (Merck Millipore, Darmstadt, Germany) following the manufacturer's instructions. Briefly, 25 µL of the sample was mixed with 200 µL of a 50:1 ratio of BCA solution and 4% cupric sulphate in a 96-well plate. After shaking for 30 seconds, the plate was incubated at 37 °C for 30 minutes. Upon completion of the incubation period, the plate was promptly transferred to a microplate reader (Infinite 200 pro, Tecan, Switzerland) and the absorbance was measured at 562 nm. The calibration standard was bovine serum albumin (0-1000 μg/mL), and all measurements were performed in triplicate.

2.6.3 Turbidity Measurement

The turbidity (τ) of the diluted and prefiltered hydrolysates with adjusted pH values (4.2, 7.0 and 10.0) was measured via UV-VIS-spectrophotometer according to Westbye *et al*. [30], and calculated using Eq. (4), where absorbance corresponds to the sample absorbance at 500 nm and the pathlength is the light path in the sample, in this case, 1 cm. All measurements were performed in triplicate.

$$\tau = \frac{absorbance}{pathlenght} \times Ln10 \quad \textbf{(4)}$$

3. Results and discussion

The hydrolysates resulting from the enzymatic hydrolysis of xylan were produced following the parameters optimized in our previous work [24], yielding XOS with various DP while limiting the generation of X1. The resulting hydrolysates contained a complex mixture of linear and branched XOS with mono- or di- 4-*O*-methyl-D-glucuronic acid (MeGluA) substituents. This composition is typical of hardwood hemicellulose, which consists of glucuronoxylan, a polysaccharide comprise of xylose residues in the main backbone substituted with MeGluA [31]. The identity of the linear and branched XOS compounds present in the hydrolysate was confirmed using LC-Q-TOF-MS and is presented in **Table S1**. Quantification of linear XOS with DP 2-6 was conducted by HPLC-ELSD as the standards were commercially available and is presented in **Table 2**.

Tubular ceramic membranes with MWCOs of 750, 450 and 200 Da in the nanofiltration range were employed to fractionate the hydrolysates into high, medium, and low DP XOS fine fractions using a crossflow filtration system. For these non-charged oligomers, the separation principle relies on size exclusion [17]. To ensure the separation between compounds by molecular sieving, a difference of at least 30 to 50 Da in molecular weight is necessary [17]. The molecular weights of XOS with DP from 2-6 range from 282.10 to 810.26 Da, with a difference of 132 Da between adjacent DPs [32].

Table 2. Quantification of linear XOS with DP 2-6 from the Beechwood xylan hydrolysate* used as feed in the crossflow filtration system. Values represent the mean ± SD, n = 10.

Compound	Molecular formula	Monoisotopic mass [Da][a]	Concentration [mg/L]
X2	$C_{10}H_{18}O_9$	282.10	224.9 ± 22.6
X3	$C_{15}H_{26}O_{13}$	414.14	269.4 ± 25.9
X4	$C_{20}H_{34}O_{17}$	546.18	160.1 ± 16.3
X5	$C_{25}H_{42}O_{21}$	678.22	94.4 ± 11.3
X6	$C_{30}H_{50}O_{25}$	810.26	35.9 ± 4.5

*Prefiltered hydrolysate using 0.45 μm membrane. [a] Exact mass calculated using the mass of the most abundant isotope of each element.

3.1 Pure water permeability of the nanofiltration membranes

The initial pure water permeate flux was measured for the pristine membranes to monitor their performance and assess the decline of the permeate flux after several cycles of hydrolysate filtration and cleaning. The pure water permeate flux of the three nanofiltration membranes was measured after 30 min of equilibration time at 25 °C and different TMP, within the safety range (**Table 1**). The linear regressions between the permeate flux and the TMP resulted in $R^2 > 0.99$, validating the linear correlation of the flux and the TMP in the range tested. The 750 Da membrane showed the highest mean permeability of 20.1 ± 7.1 LMH/bar (L m^{-2} h^{-1} bar^{-1}), followed by 17.1 ± 5.2 and 10.7 ± 1.8 LMH/bar for the 450 and 200 Da membranes, respectively.

3.2 Enzyme rejection of nanofiltration membranes

The enzyme rejection was evaluated for the three nanofiltration membranes to ensure the effective removal of enzyme present in the hydrolysates following the prefiltration step. The enzyme rejection rates (%) under standard conditions were calculated by comparing the enzyme concentrations in the feed and permeate (Eq. (3)), and presented in **Table 3.** The percentages of enzyme removed from the hydrolysates after the centrifugation step and prefiltration with the 0.45 μm membrane are also presented.

Combining these steps resulted in the removal of around 96% of the enzyme, which is expected as the enzyme used had a molecular weight of ~30 kDa [33]. The three membranes rejected more than 99% of the remaining enzyme in the hydrolysate. These results showed the effectiveness of the nanofiltration membranes to remove large molecules such as proteins. The enzyme rejection over time for each membrane was also evaluated at the different OPs (5, 10, and 15 bar) and is presented in **Fig. S2**.

Table 3. Enzyme rejection of the 750, 450, and 200 Da nanofiltration membranes at standard filtration conditions***.** Values represent the mean ± SD, n = 3.

Time [min]	Enzyme rejection [%]
Hydrolysate after centrifugation	63.8 ± 3.9
Hydrolysate after prefiltration (0.45 µm)	96.3 ± 0.4
750 Da	99.5 ± 0.2
450 Da	99.7 ± 0.1
200 Da	99.7 ± 0.1

*Filtration conditions: 25 °C, pH 4.2, operating pressure of 5 bar and 60 min filtration time.

3.3 Influence of pressure on selectivity and flux

Selection of filtration parameters that ensure a trade-off between selectivity and high flux has always been sought for efficient membrane separation processes [28]. Here, the influence of the OP on the selectivity and flux was investigated for the three nanofiltration membranes and is presented in **Figs. 2-3**.

Fig. 2A-C shows the rejection of XOS at 25 ºC, pH 4.2, filtration time of 60 min, and OPs of 5, 10 and 15 bar. At 5 and 10 bar, the membranes with MWCO of 750, 450 and 200 Da fully rejected XOS with DP > 5, DP > 4, and DP > 3, respectively. The membrane with MWCO of 200 Da was anticipated to completely reject X3 as its molecular weight, 414.14 Da, exceeds by double the MWCO of this membrane. However, the apparent MWCO of the membranes does not always match their nominal MWCO [3, 14]; it is a manufacturer approximation based on the rejection of specific compounds, *e.g.*, dextran, polyethylene glycol, and proteins [34]. Defining a precise MWCO is also limited by the fact that compounds with similar molecular masses can exhibit different molecular morphologies (linear polymer vs globular protein) [34]. The only information available for the XOS is the molecular weight, but their molecular sizes and structural conformation in solution are yet to be elucidated.

The pore size distribution of the membranes was measured by nitrogen adsorption and is presented in **Fig. S3**. The analysis revealed that the pore size distribution was mono-modal and from 31.8-86.3 Å, 29.8-79.8 Å, and 29.4-73.9 Å for the 750, 450 and 200 Da membranes, respectively. The overlapping pore size distribution among the membranes may explain the pass of X3 through the pores of the 200 Da membrane. The orientation of these elongated molecules relative to the membrane pore can also impact selectivity [25].

The rejection of X4 decreased from 100% at 10 bar to ~90% at 15 bar for the 200 Da membrane, and the rejection of X5 decreased from 100% at 10 bar to ~86% at 15 bar for the 450 Da membrane. Selectivity of membranes decreases with increasing permeate flux [34], which is the same behavior observed here when increasing the OP from 10 to 15 bar resulting in a significant decrease ($p < 0.05$) in the membrane selectivity. Therefore, to maintain the selectivity of the membranes and achieve the desired fractionation of XOS based on their DP, an OP of 10 bar or below should be used. This will allow the membranes with MWCO of 750, 450 and 200 Da to fractionate XOS into high (X2-X5), medium (X2-X4) and low (X2-X3) DPs, respectively.

Interestingly, branched XOS compounds identified in the hydrolysate feed were not detected in the permeate of any of the three membranes. Specifically, the permeate of the 750 Da membrane contained X3 and X4 with molecular weights of 414.14 and 546.18Da, respectively, while, X2MeGluA with a molecular weight of 472.14 Da, which is in the range of X3 and X4, was not detected in the permeate when analyzed by HPLC-ELSD. The structure of the molecules, therefore, appears to be playing a role in the membrane selectivity. Abundant hydroxyl moieties in the oligosaccharides lead to the formation of a hydration layer, increasing their apparent volume and affecting their dynamics [25]. The presence of substituents allows for more interaction with water molecules in the branched XOS compared to the linear XOS. Furthermore, the anomeric effect of methoxyl groups is more pronounced in aqueous solutions than that of the hydroxyl groups [35]. As a result, linear XOS might pass more easily through the membrane pores compared to XOS with methoxy groups (MeGluA substituents) of similar molecular weight.

The permeate fluxes at different OPs were evaluated and the results are presented in **Fig. 3A-C**. The hydrolysate permeate flux increased linearly with increasing TMP for the three nanofiltration membranes. The linear regressions resulted in $R^2 > 0.99$ for the 750 and 200 Da membranes, and $R^2 > 0.98$ for the 450 Da membrane. A substantial decline in the permeate flux was observed when comparing hydrolysates to water (**Table S2)**. The permeability of the 750, 450 and 200 Da membranes obtained for the hydrolysate were 7.8 ± 2.9, 5.7 ± 0.7, and 2.6 ± 0.3 LMH/bar, respectively. The decrease in the permeate flux over 60 min at the highest OP, 15 bar, was ~10%, ~9% and ~ 4% for the 750, 450 and 200 Da membranes, respectively. Whereas, at the lowest OP, 5 bar, the drop was ~4%, ~7% and ~2% for the 750, 450 and 200 Da membranes, respectively.

One of the major challenges in membrane technology is fouling, which can lead to reduced permeability and membrane selectivity [36]. Fouling is influenced by the membrane geometry, material, operating conditions, and feed composition [28]. The present study employed a crossflow filtration system with tubular ceramic membranes to mitigate this phenomenon. This configuration facilitated the parallel flow of the feed solution along the membrane surface, generating a shearing force that minimized the membrane fouling and cake layer formation [37].

A longer filtration time of 300 min (5 h) was carried out for the 750 Da membrane at 25 ºC, pH 4.2, and OP of 10 bar. No significant difference in the permeate flux drop, which remained at ~10%, was observed (**Fig. S4**). These results highlight the advantages of using a crossflow configuration and membranes with tubular geometry. Besides, the employed membranes were ceramic membranes with high mechanical strength and chemical resistance that allowed them to be cleaned and reused between filtrations.

Efficient membrane separation processes require a balance between selectivity and high flux. While the highest permeate flux among the three membranes was observed at an OP of 15 bar, the selectivity of the 450 and 200 Da membranes was compromised at this pressure. Consequently, to maintain both effective fractionation of XOS into three distinct DP ranges and a high flux rate, an OP of 10 bar was selected for subsequent experiments focusing on investigating the influence of hydrolysate pH.

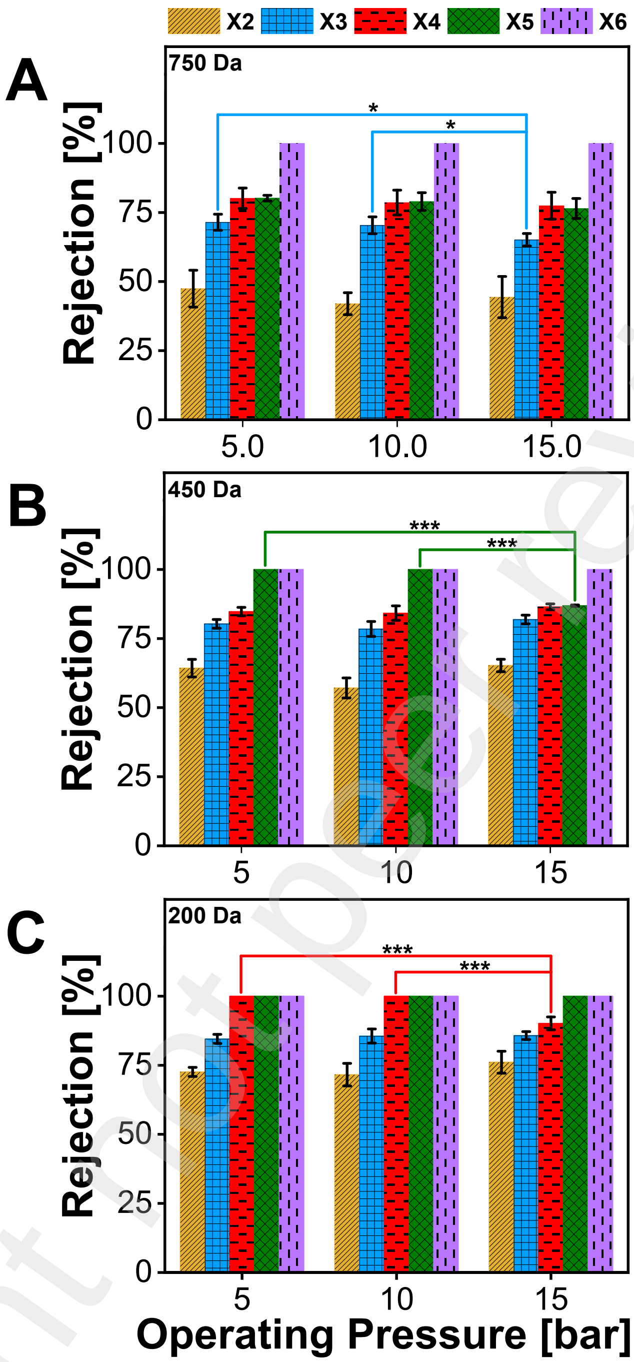

Fig. 2. (A-C): Rejection of xylooligosaccharides with degrees of polymerisation from 2 to 6 (X2 – X6) at 25 ºC, pH 4.2, 60 min filtration time versus operating pressure using membranes with the molecular weight cut-offs (MWCOs) of (A) 750 Da, (B) 450 Da, and (C) 200 Da. Values represent the mean ± SD, $n = 3$, *$p < 0.05$, **$p < 0.01$, ***$p < 0.005$ (obtained by Student's t-test).

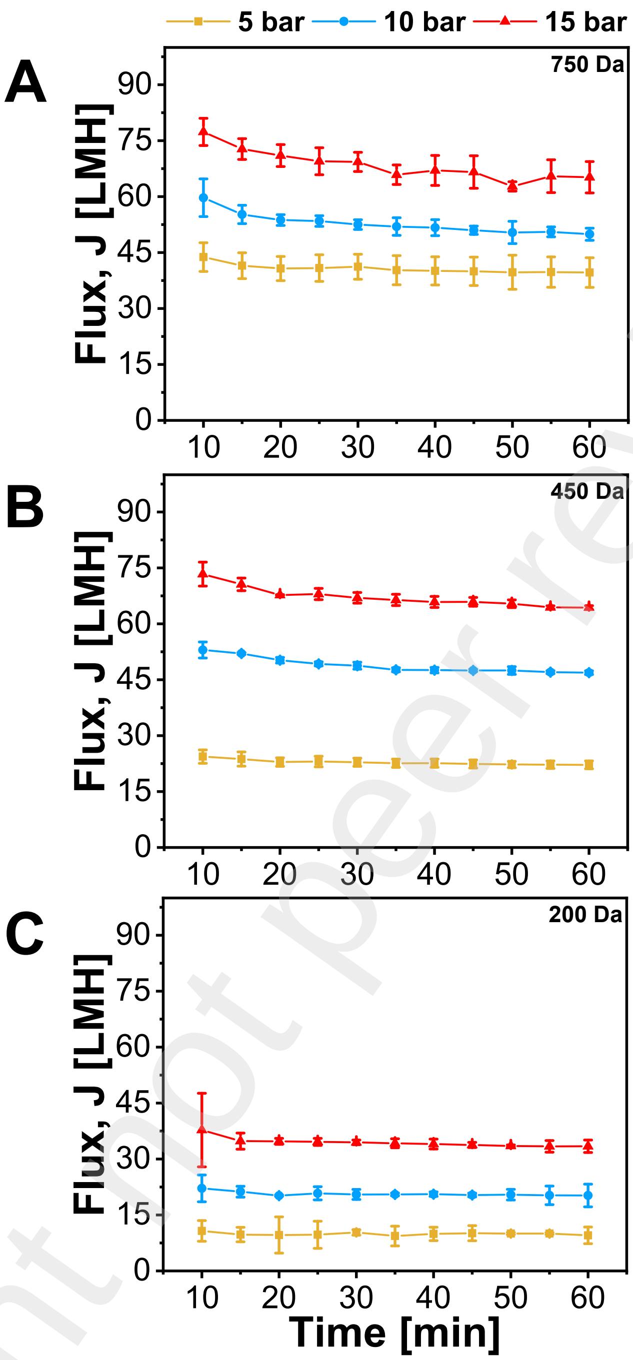

Fig. 3. (A-C): Hydrolysate permeate flux at 25 ºC, pH 4.2, 60 min filtration time versus operating pressures using membranes with molecular weight cut-offs (MWCOs) of (A) 750 Da, (B) 450 Da, and **(**C) 200 Da.

3.4 Influence of pH on selectivity and flux

The influence of pH on the rejection of linear XOS with DP 2-6 and permeate flux was investigated and the results are presented in **Figs. 4-5**. **Fig. 4A-C** shows the rejection percentages of XOS at three different hydrolysate pH values of 4.2, 7.0 and 10.0 at 25 ºC, OP of 10 bar, and filtration time of 60 min. A general trend of decreasing rejection of XOS with DP 2 to 5 was observed when increasing the hydrolysate pH from 4.2 to 7.0 and 10.0. For the 750 Da membrane **(Fig. 4A)**, significant decreases ($p < 0.05$) in the rejection of X3 (from 70% to 43%) and X5 (from 79% to 69%) were observed when increasing the pH from 4.2 to 10.0. The same trend was also observed for the 450 Da membrane **(Fig. 4B)**, the rejection of X2, X3, and X4 decreased significantly ($p < 0.05$) with increasing hydrolysate pH. The selectivity of the 200 Da membrane was also pH-dependent (**Fig. 4C**). At pH 4.2, X4 was completely rejected, whereas at pH 7.0 and 10.0, the rejection decreased to 87% and 84%, respectively. Domingos *et al*. [27], observed similar behavior in the rejection of X1, where increasing the pH from 5.2 to 9.0 reduced the rejection from ~90% to ~40%.

The permeate fluxes at different hydrolysate pH values of 4.2, 7.0 and 10.0 were also evaluated and presented in **Fig. 5A-C**. For all three nanofiltration membranes, a change in pH value from 4.2 to 7.0 and 10.0 resulted in an increase in the hydrolysate permeate flux. On the other hand, the decline in the permeate flux over 60 min at pH 4.2 was ~10% for the 750 and 450 Da membranes and ~5% for the 200 Da membrane. Whereas, at pH 10 this drop was ~8%, ~5% and ~3% for the 750, 450 and 200 Da membranes, respectively.

The highest permeate flux and minimal decline in flux over time were observed when the hydrolysate was at pH values of 7.0 and 10.0 for all three membranes. However, the selectivity of the 200 Da membrane decreased significantly at neutral and basic pH levels. In the case of the 450 and 750 Da membranes, the same XOS compounds were rejected under these pH conditions. To avoid resorting to harsh conditions (pH 10.0) while still increasing the concentration of the desired XOS in the permeate, a pH of 7.0 is recommended for the 450 and 750 Da membranes. In contrast, a pH of 4.2 is necessary for the 200 Da membrane to ensure complete rejection of X4 and maintain the fractionation of XOS into low, medium and high DP ranges.

The observed trends in **Figs. 4-5**, namely the reduction in XOS rejection and the rise in permeate flux with increasing pH, can be attributed to the self-aggregation tendencies of these oligomers in solution, particularly at lower pH levels [38, 39]. It has been suggested that the aggregation mechanism of glucuronoxylans is due to the hydrogen bonding between linear portions of polysaccharide chains [38, 40] and the interactions between hydrophobic substituents bonded to the polysaccharide chain [38, 41, 42]. The turbidity of the hydrolysate at different pH values was evaluated following the method described by Westbye *et al*. [30]. **Fig. 6** presents the hydrolysate turbidity measured at 25 °C and pH values of 4.2, 7.0 and 10.0. A significant reduction ($p < 0.005$) in the turbidity was observed when increasing the pH from 4.2 to 10.0. Hu *et al*. [39], also reported a similar trend using glucuronoxylans. Therefore, it can be inferred that acidic media favors intra- and intermolecular hydrogen bonding and induced the aggregation of XOS. It was also reported that the aggregation of glucuronoxylans depends on their chemical structure rather than their molecular weight [43]. Hence, the same aggregation behavior was observed in the current study, despite the use of lower molecular weight oligomers.

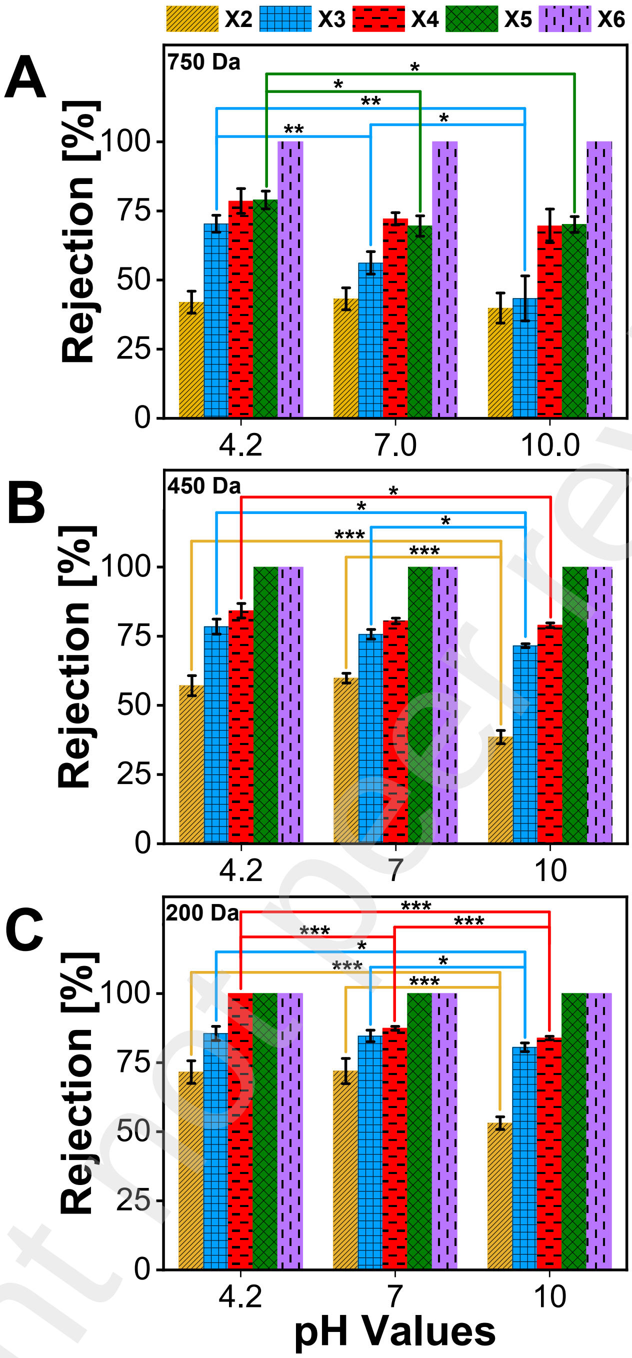

Fig. 4. (A-C): Rejection of xylooligosaccharides with degrees of polymerisation from 2 to 6 (X2 – X6) at 25 ºC, 10 bar, 60 min filtration time versus hydrolysate pH using membranes with molecular weight cut-offs (MWCOs) of (A) 750 Da, (B) 450 Da, and (C) 200 Da. Values represent the mean ± SD, $n = 3$, $*p < 0.05$, $**p < 0.01$, $***p < 0.005$ (obtained by Student's t-test).

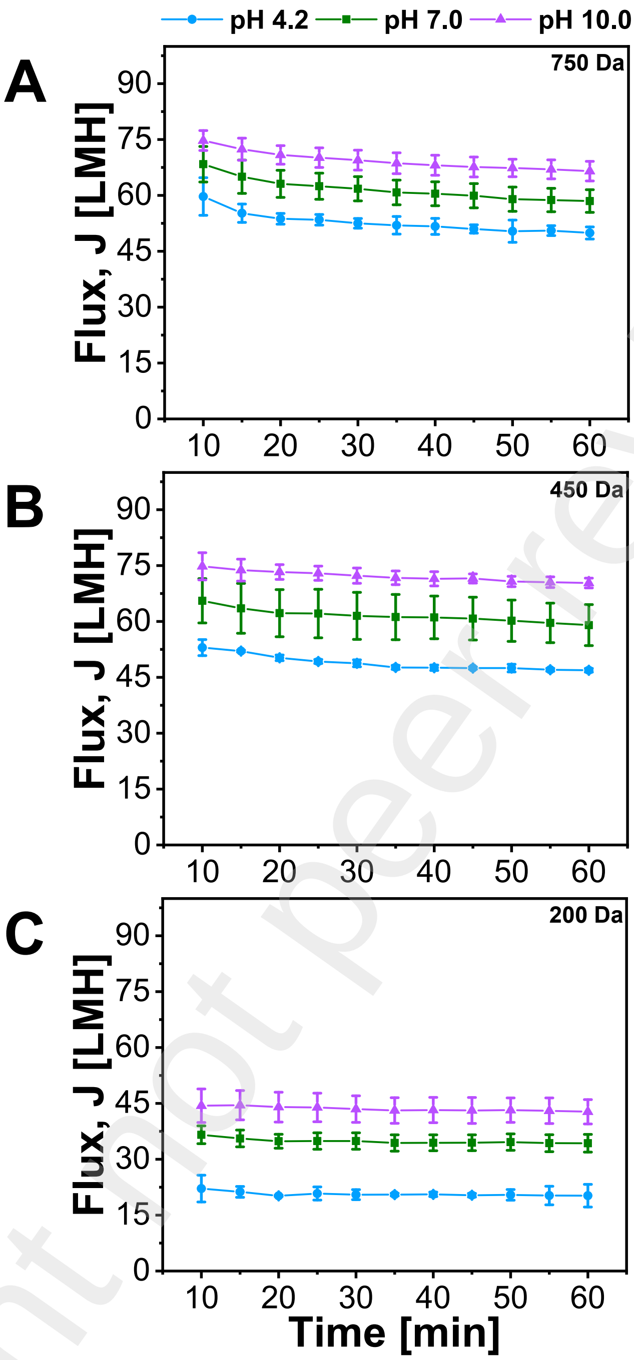

Fig. 5. (A-C): Hydrolysate permeate flux at 25 ºC, 10 bar, 60 min filtration time versus hydrolysate pH using membranes with the molecular weight cut-offs (MWCOs) of (A) 750 Da, (B) 450 Da, and **(**C) 200 Da.

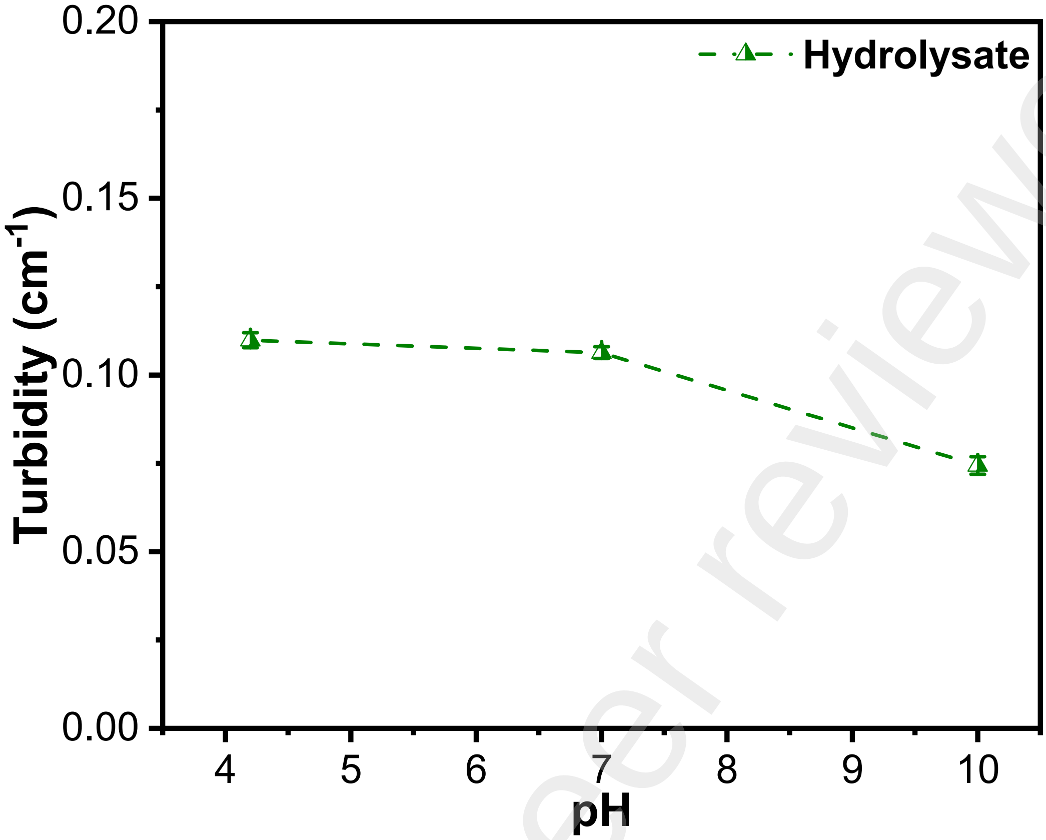

Fig. 6. Influence of the pH on the turbidity of hydrolysates. Measurements conducted at 25 °C and hydrolysate pH values of 4.2, 7.0, and 10.0.

The rejection of XOS and the permeate flux obtained for the 750, 450, and 200 Da membranes at the different OPs and hydrolysate pH values were consistent over different cycles of hydrolysate filtration and CIP protocol. In addition, pure water fluxes were also measured following the CIP for the three membranes after 30 min of equilibration time at 25 °C, OP of 5 bar, and the results are presented in **Fig. S1.** The change in the permeate flux after 10 cycles was less than 10% for the three membranes. This is evidence of the CIP protocol being effective in recovering the membrane performance, as well as the robustness of the membranes after continuous operation. These are critical aspects to consider when scaling up the separation method for integration into the existing industrial processes.

4. Conclusion

Nanofiltration employing membranes with molecular weight cut-offs of 750, 450 and 200 Da proved suitable to separate branched XOS from linear XOS, as well as fractionate linear XOS with DP 2-5, DP 2-4 and DP 2-3, respectively. The effects of operating pressure and hydrolysate pH on the rejection of XOS and permeate flux of the nanofiltration membranes was investigated. An operating pressure of 10 bar provided the best trade-off between selectivity and productivity across the three membranes. XOS rejection decreased as hydrolysate pH increased, with the highest rejection observed at pH 4.2 and the lowest at pH 10.0. The turbidity of the hydrolysates also decreased with increasing pH, indicating a reduction in the aggregation of XOS. Having a clear understanding of the influence of pressure and pH on the rejection of XOS will inform the scale-up of this technology.

The robustness of the membranes after continuous operation and the effectiveness of the cleaning-in-place protocol were demonstrated with pure water flux variation below 10% after 10 cycles for each membrane. These aspects are vital considerations to integrate this separation method into existing industrial processes.

Achieving selective separation of XOS using membrane technology relies on a comprehensive understanding of the behavior of these oligomers in solution, especially molecular sizes, agglomeration mechanisms, and the conditions that govern these effects. The implementation of ceramic nanofiltration membranes appears to be a highly efficient and versatile separation technique that can be easily scaled up and may be applicable to the processing of other functional biomolecules such as galactooligosaccharides, and fructooligosaccharides, among others.

CRediT authorship contribution statement

Gloria Lizeth Díaz-Arenas: Conceptualization, Methodology, Investigation, Formal analysis, Data curation, Writing - original draft. **Huy Quoc Hoang:** Investigation. **Hans Cainglet:** Writing – review & editing. **M. Munir Sadiq:** Supervision, Writing – review & editing. **Gil Garnier:** Supervision, Funding acquisition, Writing – review & editing. **Joanne Tanner:** Conceptualization, Supervision, Writing – review & editing.

Declaration of Competing Interest

The authors declare that they have no known competing financial interests or personal relationships that could have appeared to influence the work reported in this paper.

Acknowledgements

The authors would like to thank Phillip Holt for the assistance in carrying out the LC-Q-TOF-MS at the Chemistry Instrument Facility and Service, School of Chemistry, Monash University.

Funding

This work was supported by the ARC Industrial Transformation Research Hub for Processing Advanced Lignocellulosics Products (PALs) (Grant: ARC IH170100020), and the Australian Government Research Training Program (RTP).

References

[1] A. Moure, P. Gullón, H. Domínguez, J.C. Parajó, Advances in the manufacture, purification and applications of xylo-oligosaccharides as food additives and nutraceuticals, Process Biochem. 41(9) (2006) 1913-1923. https://doi.org/10.1016/j.procbio.2006.05.011.

[2] A.K. Samanta, N. Jayapal, C. Jayaram, S. Roy, A.P. Kolte, S. Senani, M. Sridhar, Xylooligosaccharides as prebiotics from agricultural by-products: Production and applications, Bioact. Carbohydr. Diet. Fibre 5(1) (2015) 62-71. https://doi.org/10.1016/j.bcdf.2014.12.003.

[3] D. Nabarlatz, C. Torras, R. Garciavalls, D. Montane, Purification of xylo-oligosaccharides from almond shells by ultrafiltration, Sep. Purif. Technol. 53(3) (2007) 235-243. https://doi.org/10.1016/j.seppur.2006.07.006.

[4] M.A. Kabel, L. Kortenoeven, H.A. Schols, A.G.J. Voragen, In Vitro Fermentability of Differently Substituted Xylo-oligosaccharides, J. Agric. Food. Chem. 50(21) (2002) 6205-6210. https://doi.org/10.1021/jf020220r.

[5] A. Palaniappan, V.G. Balasubramaniam, U. Antony, Prebiotic potential of xylooligosaccharides derived from finger millet seed coat, Food Biotechnol. 31(4) (2017) 264-280. https://doi.org/10.1080/08905436.2017.1369433.

[6] R. Deutschmann, R.F.H. Dekker, From plant biomass to bio-based chemicals: Latest developments in xylan research, Biotechnol. Adv. 30(6) (2012) 1627-1640. https://doi.org/10.1016/j.biotechadv.2012.07.001.

[7] M. Gonçalves De Oliveira, M. Bruno Soares Forte, T. Teixeira Franco, A serial membrane-based process for fractionation of xylooligosaccharides from sugarcane straw hydrolysate, Sep. Purif. Technol. (2021) 119285. https://doi.org/10.1016/j.seppur.2021.119285.

[8] A.A. Aachary, S.G. Prapulla, Xylooligosaccharides (XOS) as an Emerging Prebiotic: Microbial Synthesis, Utilization, Structural Characterization, Bioactive Properties, and Applications, Compr. Rev. Food Sci. Food Saf. 10(1) (2011) 2-16. https://doi.org/10.1111/j.1541-4337.2010.00135.x.

[9] Q. Qing, H. Li, R. Kumar, C.E. Wyman, Xylooligosaccharides Production, Quantification, and Characterization in Context of Lignocellulosic Biomass Pretreatment, Aqueous Pretreatment of Plant Biomass for Biological and Chemical Conversion to Fuels and Chemicals, Charles E. Wyman, Chichester, 2013, pp. 391-415.

[10] O. Akpinar, O. Ak, A. Kavas, U. Bakir, L. Yilmaz, Enzymatic Production of Xylooligosaccharides from Cotton Stalks, J. Agric. Food. Chem. 55(14) (2007) 5544-5551. https://doi.org/10.1021/jf063580d.

[11] L. Ansaloni, L. Deng, Advances in polymer-inorganic hybrids as membrane materials, Recent Developments in Polymer Macro, Micro and Nano Blends, Woodhead Publishing, Duxford, 2017, pp. 163-206.

[12] P. Gullón, M.J. González-Muñoz, H. Domínguez, J.C. Parajó, Membrane processing of liquors from Eucalyptus globulus autohydrolysis, J. Food Eng. 87(2) (2008) 257-265. https://doi.org/10.1016/j.jfoodeng.2007.11.032.

[13] K. Swennen, C. Courtin, B. Vanderbruggen, C. Vandecasteele, J. Delcour, Ultrafiltration and ethanol precipitation for isolation of arabinoxylooligosaccharides with different structures, Carbohydr. Polym. 62(3) (2005) 283-292. https://doi.org/10.1016/j.carbpol.2005.08.001.

[14] A. Córdova, C. Astudillo, A. Illanes, Membrane Technology for the Purification of Enzymatically Produced Oligosaccharides, Separation of Functional Molecules in Food by Membrane Technology, Academic Press, London, 2019, pp. 113-153.
[15] R. Vegas, S. Luque, J.R. Alvarez, J.L. Alonso, H. Domínguez, J.C. Parajó, Membrane-Assisted Processing of Xylooligosaccharide-Containing Liquors, J. Agric. Food. Chem. 54(15) (2006) 5430-5436. https://doi.org/10.1021/jf060525w.
[16] H. Zhao, X. Hua, R. Yang, L. Zhao, W. Zhao, Z. Zhang, Diafiltration process on xylo-oligosaccharides syrup using nanofiltration and its modelling, Int. J. Food Sci. Tech. 47(1) (2012) 32-39. https://doi.org/10.1111/j.1365-2621.2011.02803.x.
[17] A. Kruschitz, B. Nidetzky, Downstream processing technologies in the biocatalytic production of oligosaccharides, Biotechnol. Adv. 43 (2020). https://doi.org/10.1016/j.biotechadv.2020.107568.
[18] M. Pinelo, G. Jonsson, A.S. Meyer, Membrane technology for purification of enzymatically produced oligosaccharides: Molecular and operational features affecting performance, Sep. Purif. Technol. 70(1) (2009) 1-11. https://doi.org/10.1016/j.seppur.2009.08.010.
[19] B. Van der Bruggen, M. Mänttäri, M. Nyström, Drawbacks of applying nanofiltration and how to avoid them: A review, Sep. Purif. Technol. 63(2) (2008) 251-263. https://doi.org/10.1016/j.seppur.2008.05.010.
[20] A. Al-Amoudi, Effect of chemical cleaning agents on virgin nanofiltration membrane as characterized by positron annihilation spectroscopy, Sep. Purif. Technol. 110 (2013) 51-56. https://doi.org/10.1016/j.seppur.2013.02.005.
[21] X. Shi, G. Tal, N.P. Hankins, V. Gitis, Fouling and cleaning of ultrafiltration membranes: A review, J. Water Process. Eng. 1 (2014) 121-138. https://doi.org/10.1016/j.jwpe.2014.04.003.
[22] B.F.K. Kingsbury, K. Li, A morphological study of ceramic hollow fibre membranes, J. Membr. Sci. 328(1-2) (2009) 134-140. https://doi.org/10.1016/j.memsci.2008.11.050.
[23] G.L. Baruah, A. Nayak, G. Belfort, Scale-up from laboratory microfiltration to a ceramic pilot plant: Design and performance, J. Membr. Sci. 274(1) (2006) 56-63. https://doi.org/https://doi.org/10.1016/j.memsci.2005.07.046.
[24] G.L. Díaz-Arenas, L. Lebanov, E. Sanz Rodríguez, M. Munir Sadiq, B. Paull, G. Garnier, J. Tanner, Chemometric Optimisation of Enzymatic Hydrolysis of Beechwood Xylan to Target Desired Xylooligosaccharides, Bioresour. Technol. (2022) 127041. https://doi.org/10.1016/j.biortech.2022.127041.
[25] V. Aguirre Montesdeoca, J. Bakker, R.M. Boom, A.E.M. Janssen, A. Van der Padt, Ultrafiltration of non-spherical molecules, J. Membr. Sci. 570-571 (2019) 322-332. https://doi.org/10.1016/j.memsci.2018.10.053.
[26] G.Q. Chen, A. Artemi, J. Lee, S.L. Gras, S.E. Kentish, A pilot scale study on the concentration of milk and whey by forward osmosis, Sep. Purif. Technol. 215 (2019) 652-659. https://doi.org/10.1016/j.seppur.2019.01.050.
[27] J.M.B. Domingos, A.R.S. Teixeira, S. Dupoiron, F. Allais, M.-L. Lameloise, Simultaneous recovery of ferulic acid and sugars from wheat bran enzymatic hydrolysate by diananofiltration, Sep. Purif. Technol. 242 (2020) 116755. https://doi.org/10.1016/j.seppur.2020.116755.
[28] M. Mulder, Basic principles of membrane technology, First ed., Kluwer Academic Publishers, Dordrecht, 1991.
[29] D.H. Tran, M. Ulbricht, Cellulose-cellulose composite membranes for ultrafiltration, J. Membr. Sci. 672 (2023) 121426. https://doi.org/10.1016/j.memsci.2023.121426.

[30] P. Westbye, T. Köhnke, W. Glasser, P. Gatenholm, The influence of lignin on the self-assembly behaviour of xylan rich fractions from birch (Betula pendula), Cellulose 14(6) (2007) 603-613. https://doi.org/10.1007/s10570-007-9178-0.

[31] L. Santibáñez, C. Henríquez, R. Corro-Tejeda, S. Bernal, B. Armijo, O. Salazar, Xylooligosaccharides from lignocellulosic biomass: A comprehensive review, Carbohydr. Polym. 251 (2021) 117118. https://doi.org/10.1016/j.carbpol.2020.117118.

[32] E. Sanz Rodríguez, G.L. Díaz-Arenas, S. Makart, D. Ghosh, A.F. Patti, G. Garnier, J. Tanner, B. Paull, Determination of xylooligosaccharides produced from enzymatic hydrolysis of beechwood xylan using high-performance anion-exchange chromatography tandem mass spectrometry, J. Chromatogr. A 1666 (2022) 462836. https://doi.org/10.1016/j.chroma.2022.462836.

[33] J.A. Linares-Pasten, A. Aronsson, E.N. Karlsson, Structural Considerations on the Use of Endo-Xylanases for the Production of prebiotic Xylooligosaccharides from Biomass, Curr. Protein Peptide Sci. 19(1) (2017) 1-1. https://doi.org/10.2174/1389203717666160923155209.

[34] R. Singh, Chapter 1 - Introduction to membrane technology, in: R. Singh (Ed.), Hybrid Membrane Systems for Water Purification, Elsevier Science, Amsterdam, 2005, pp. 1-56.

[35] S.J. Angyal, The Composition and Conformation of Sugars in Solution, Angewandte Chemie, Angew. Chem., Int. Ed. Engl. 8(3) (1969) 157-166. https://doi.org/10.1002/anie.196901571.

[36] C. Li, W. Sun, Z. Lu, X. Ao, S. Li, Ceramic nanocomposite membranes and membrane fouling: A review, Water Res. 175 (2020) 115674. https://doi.org/10.1016/j.watres.2020.115674.

[37] X. Du, Y. Shi, V. Jegatheesan, I.U. Haq, A Review on the Mechanism, Impacts and Control Methods of Membrane Fouling in MBR System, Membranes 10(2) (2020) 24. https://doi.org/10.3390/membranes10020024.

[38] Å. Linder, R. Bergman, A. Bodin, P. Gatenholm, Mechanism of Assembly of Xylan onto Cellulose Surfaces, Langmuir 19(12) (2003) 5072-5077. https://doi.org/10.1021/la0341355.

[39] G. Hu, J. Hu, H. Chen, S. Song, F. Chu, Influence of pH and Ionic Strength on the Aggregation Behaviors of Xylan Rich Hemicelluloses with Alkaline Lignins, Bioresources. 16(4) (2021) 7608-7622. https://doi.org/10.15376/biores.16.4.7608-7622.

[40] F. Mora, K. Ruel, J. Comtat, J.-P. Joseleau, Aspect of native and redeposited xylans at the surface of cellulose microfibrils, Holzforschung. 40 (1986) 85-91. https://doi.org/10.1515/hfsg.1986.40.2.85.

[41] A. Esker, U. Becker, S. Jamin, S. Beppu, S. Renneckar, W. Glasser, Self-Assembly Behavior of Some Co-and Heteropolysaccharides Related to Hemicelluloses, Hemicelluloses: Science and Technology, American Chemical Society, Washington, DC, 2003, pp. 198-219.

[42] P. Westbye, C. Svanberg, P. Gatenholm, The effect of molecular composition of xylan extracted from birch on its assembly onto bleached softwood kraft pulp, Holzforschung. 60 (2006) 143–148. https://doi.org/10.1515/HF.2006.023.

[43] B. Saake, T. Kruse, J. Puls, Investigation on molar mass, solubility and enzymatic fragmentation of xylans by multi-detected SEC chromatography, Bioresour. Technol. 80(3) (2001) 195-204. https://doi.org/10.1016/S0960-8524(01)00089-X.

Supplementary Data

Unlocking the Potential of Xylooligosaccharides: Nanofiltration for Efficient Fractionation of Hardwood Hydrolysates

Gloria Lizeth Diaz-Arenas [a], Huy Quoc Hoang [a], Hans Cainglet [a], M. Munir Sadiq [b], Gil Garnier [a], Joanne Tanner [a]*

[a] *Bioresource Processing Research Institute of Australia (BioPRIA), Department of Chemical and Biological Engineering, Monash University, Clayton, VIC 3800, Australia*

[b] *Manufacturing, CSIRO, Clayton, VIC 3169, Australia*

*Joanne Tanner (Corresponding Author); **E-mail address:** joanne.tanner@monash.edu

Full postal address: *Woodside Building for Technology and Design, Room 328, 20 Exhibition Walk, Monash University, Clayton, VIC, Australia*

Appendix A

Instrumental LC-Q-TOF-MS

An Agilent UPLC 1260 system coupled to Accurate-Mass Quadrupole Time-of-Flight 6540 mass spectrometer Q-TOF-MS (Agilent Technologies, Santa Clara, USA), equipped with a Dual AJS ESI source operating in negative mode. The ESI source was set at negative ion mode with a capillary drying gas temperature of 300 °C, an ion spray voltage of 300 kV and a sheath gas flow rate of 10 l/min. Full-scan high resolution scanning range was 50–1800 m/z. After sample 2-fold dilution, 10 µL were injected via a vial-sampler (controlled temperature at 10 °C) onto a Shodex HILICpak VG-50 (4.6 × 150 mm) chromatographic column (Showa Denko America, New York, USA). The mobile phases used in the separation were aqueous ammonia 0.1% v/v [solvent A] and acetonitrile [solvent B]. The target analytes were separated at 50 °C, at a flow rate of 0.7 mL min^{-1} in gradient elution mode as follows: 80% [B] held 1 min, 80% to 65% [B] in 18 min, 65% back to 80% [B] in 6 min, 80% [B] held 11 min. The total run time was 35 min including 11 min equilibration step before the next injection. Data were acquired and treated by means of Agilent MassHunter Software. The hydrolysate composition is presented in **Table S1.**

Table S1. Qualitative composition of the diluted and prefiltered hydrolysate* including name abbreviations, molecular formulae, and theoretical monoisotopic masses.

Compound	Molecular formula	Monoisotopic mass (Da)[a]
X1	$C_5H_{10}O_5$	150.0528
X2	$C_{10}H_{18}O_9$	282.0951
X3	$C_{15}H_{26}O_{13}$	414.1374
X4	$C_{20}H_{34}O_{17}$	546.1797
X5	$C_{25}H_{42}O_{21}$	678.222
X6	$C_{30}H_{50}O_{25}$	810.2643
X7	$C_{35}H_{58}O_{29}$	942.3065
X8	$C_{40}H_{66}O_{33}$	1074.3488
X9	$C_{45}H_{74}O_{37}$	1206.3911
X2MeGluA	$C_{17}H_{28}O_{15}$	472.1429
X3MeGluA	$C_{22}H_{36}O_{19}$	604.1852
X4MeGluA	$C_{27}H_{44}O_{23}$	736.2275
X5MeGluA	$C_{32}H_{52}O_{27}$	868.2697
X6MeGluA	$C_{37}H_{60}O_{31}$	1000.312
X7MeGluA	$C_{42}H_{68}O_{35}$	1000.312
X8MeGluA	$C_{47}H_{76}O_{39}$	1264.3966
X9MeGluA	$C_{52}H_{84}O_{43}$	1396.4389
X10MeGluA	$C_{57}H_{92}O_{47}$	1528.4811
X11MeGluA	$C_{62}H_{100}O_{51}$	1660.5234
X7MeGluA2	$C_{49}H_{78}O_{41}$	1322.4021
X8MeGluA2	$C_{54}H_{86}O_{45}$	1454.4444
X9MeGluA2	$C_{59}H_{94}O_{49}$	1586.4866

*Prefiltered hydrolysate using 0.45 μm membrane. [a] Exact mass calculated using the mass of the most abundant isotope of each element.

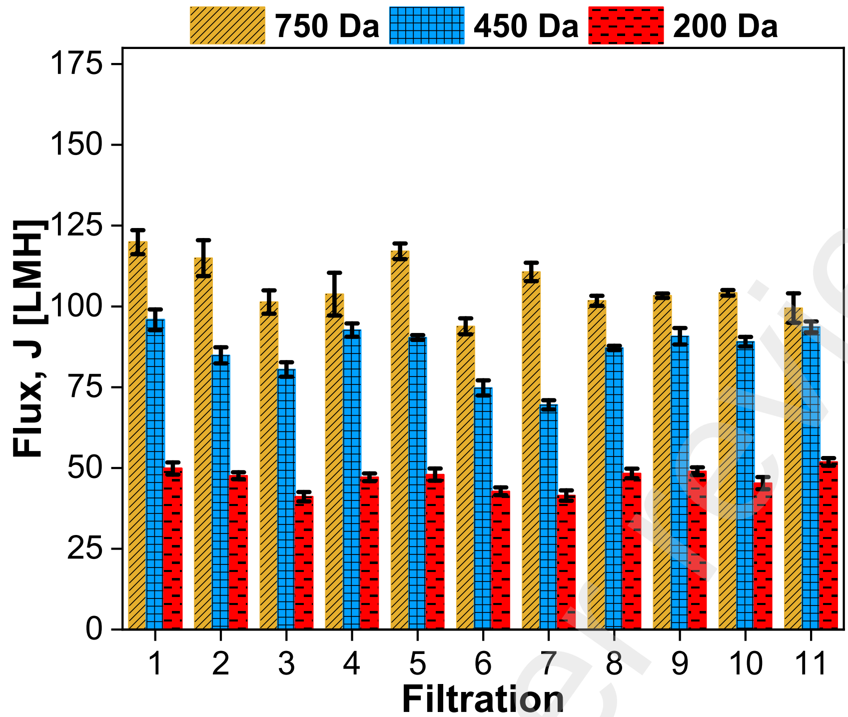

Fig. S1. Pure water permeate flux measured at standard conditions of 25 ºC, OP of 5 bar, and 30 min for the nanofiltration membranes with the molecular weight cut-offs of 750 Da, 450 Da, and 200 Da; Filtration 1 indicates the pure water permeate flux of the pristine membranes and the rest of the filtrations refer to the pure water permeate fluxes after filtration of hydrolysates and cleaning-in-place protocol.

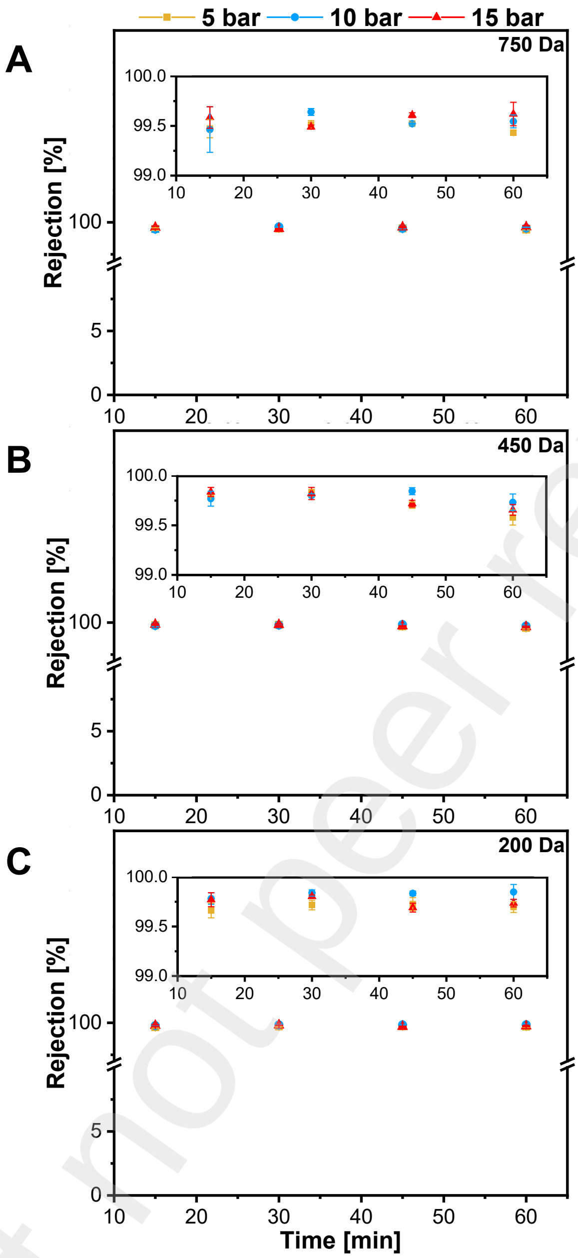

Fig. S2. Enzyme rejection measured at standard filtration conditions of 25 °C, pH 4.2, OP of 5, 10 and 15 bar, 60 min filtration time and 15 min sampling frequency using membranes with the molecular weight cut-offs of (A) 750, (B) 450, and (C) 200 Da nanofiltration membranes.

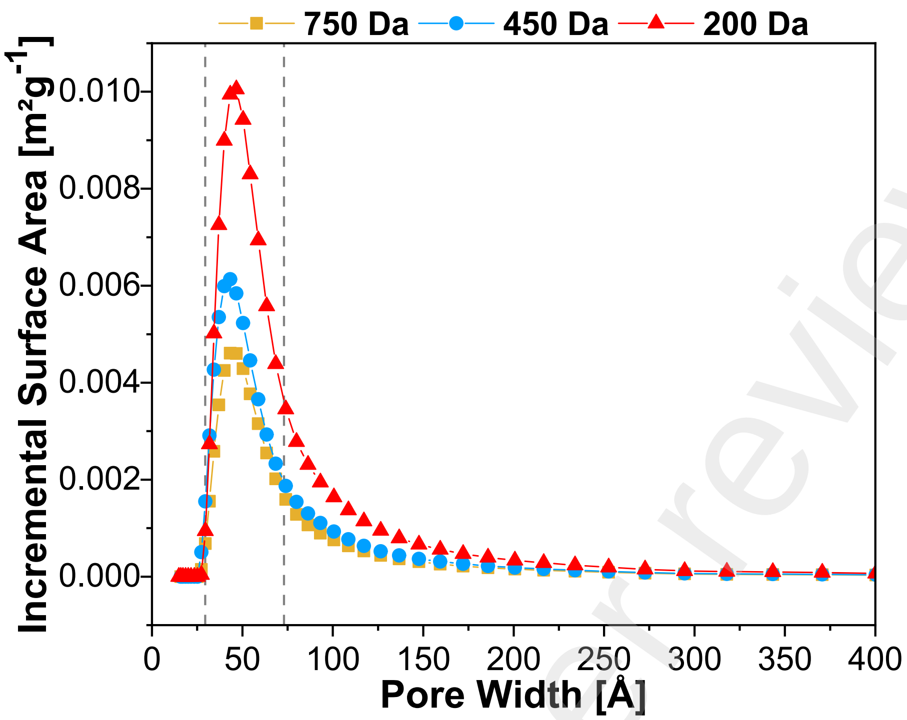

Fig. S3. Pore size distribution of the 750, 450, and 200 Da membranes determined by measuring nitrogen (N_2) adsorption isotherms at 77 K in a liquid-nitrogen bath and calculated using Micromeritics software. The measurements were performed on Micromeritics Tristar II instrument.

Table S2. Permeability (L_p) of the membranes with the molecular weight cut-offs of 750, 450, and 200 Da to water and to the hydrolysate measured at 25 °C, pH, and operating pressure of 5 bar.

Membrane [MWCO]	Permeability [LHM/bar]	
	Water	Hydrolysate
750 Da	20.1 ± 7.1	7.8 ± 2.9
450 Da	17.1 ± 5.2	5.7 ± 0.7
200 Da	10.7 ± 1.8	2.6 ± 0.3

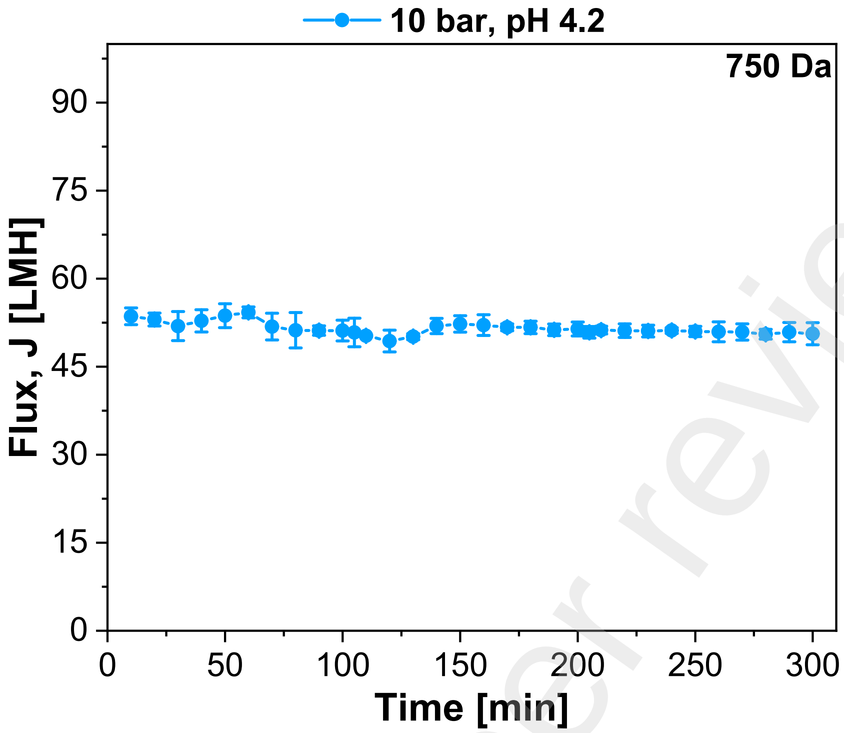

726
727 **Fig. S4.** Hydrolysate permeate flux measured at 25 ºC, pH 4.2, 10 bar, 300 min
728 filtration time using the membrane with molecular weight cut-off of 750 Da.